ARTICLE

Fabrication of Ordered NiO Coated Si Nanowire Array Films as Electrodes for a High Performance Lithium Ion Battery

M. C. Qiu, L. W. Yang,* X. Qi, Jun Li, and J. X. Zhong*

Institute for Quantum Engineering and Micro-Nano Energy Technology and Faculty of Materials and Optoelectronic Physics, Xiangtan University, Hunan 411105, P. R. China

ABSTRACT Highly ordered NiO coated Si nanowire array films are fabricated as electrodes for a high performance lithium ion battery via depositing Ni on electroless-etched Si nanowires and subsequently annealing. The structures and morphologies of as-prepared films are characterized by X-ray diffraction, scanning electron microscopy, and transmission electron microscopy. When the potential window versus lithium was controlled, the coated NiO can be selected to be electrochemically active to store and release Li^+ ions, while highly conductive crystalline Si cores function as nothing more than a stable mechanical support and an efficient electrical conducting pathway. The hybrid nanowire array films exhibit superior cyclic stability and reversible capacity compared to that of NiO nanostructured films. Owing to the ease of large-scale fabrication and superior electrochemical performance, these hybrid nanowire array films will be promising anode materials for high performance lithium-ion batteries.

KEYWORDS: lithium-ion batteries • electrochemical performance • hybrid nanowire array • NiO • Si • electroless-etching

1. INTRODUCTION

The increasing demand for high-energy-density, long-cycle-life, and low-environmental-impact power sources in the fields of portable electronic devices, electric vehicles, implantable medical devices, etc. has stimulated intensive exploration of new electrode materials for rechargeable lithium-ion batteries (1−4). Among various alternative anode materials being studied, transition metal oxides (MO_x, M = Ni, Fe, Co, Cu, etc.) have attracted great interest due to their high theoretical capacity, safety, environmental benignity, and low cost (3−8). For example, when NiO is used as the anode material for Li ion batteries, its theoretical capacity is about 718 mAh/g, which is much higher than that of the commercial graphite anode material (372 mAh/g) (6, 8). However, the practical use of these materials in lithium-ion batteries has been frustrated due to their poor electrical conductivity and large volume and structure change during the lithium uptake/release process. To overcome these issues, various nanostructured materials of these electrodes with controlled size, crystallinity, and chemical composition were designed (8−18). Besides the large contact area with electrolyte and the facile strain relaxation during structure and volume change, nanostructured materials shorten lithium ion diffusion length, leading to enhanced power density compared to bulk counterparts. It has been reported that NiO nanowalls show excellent capacity retention and high rate performance during cycling (16). Unfortunately, the conductivity of these nanostructured electrodes remains an existing issue. Recently, novel hybrid nanostructured materials such as crystalline−amorphous core−shell silicon nanowires and carbon−silicon core−shell nanowires used as the anode material for lithium ion batteries displayed excellent electrochemical performance (19−23). In these hybrid nanostructured materials, crystalline Si cores function as a stable mechanical support and an efficient electrical conducting pathway, while amorphous Si or carbon shells having large contact area with electrolyte as active materials store and release Li^+ ions. It can be imaged that similar hybrid nanostructures would also significantly improve the electrochemical performance of MO_x anode materials. Very recently, Reddy et al. reported that coaxial manganese oxide/carbon nanotube (CNT) arrays used as cathodes in a lithium battery had excellent cyclic stability and reversible capacity resulted from the hybrid nature of the electrodes with improved electronic conductivity and dual mechanism of lithium storage compared to template grown MnO_2 nanotubes (22). In this investigation, we fabricated highly ordered NiO coated Si nanowire array films via depositing Ni on electroless-etched Si nanowires and subsequently annealing. Their superior electrochemical performance is also demonstrated.

2. EXPERIMENTAL SECTION

2.1. Preparation of NiO Coated Si Nanowire Array Films. The fabrication of highly ordered NiO coated Si nanowire array films include three processes as follows. First, Si nanowire array films of 10 mm × 10 mm × 57 μm were prepared using metal catalytic etching of single-crystal high (0.008−0.02 $\Omega \cdot$ cm) or low (1−10 $\Omega \cdot$ cm) doped *p*-type silicon (100) wafers (24−27). Before the etching reaction, the cleaned wafer was coated with a thin corrosion-resistant plastic layer around the edge of each square and on the back as an etch mask so that the contacts could be made on planar Si. Then, it was immersed into an

* Corresponding author. E-mail: ylwxtu@xtu.edu.cn (L.W.Y.); zhong.xtu@gmail.com (J.X.Z.).
Received for review August 26, 2010 and accepted November 1, 2010
DOI: 10.1021/am100791z

Published on Web 11/15/2010

etching solution containing 4.8 M HF and 0.005 M $AgNO_3$ for 1 min to precipitate silver particles and was subsequently transferred to another etching solution containing 4.8 M HF and 0.3 M H_2O_2 at 323 K to undergo a metal catalytic etching. After 45 min, the wafer was cleaned with dilute HNO_3 (1:1 V/V) for 1 h to remove the residual Ag catalyst and rinsed three times with deionized water to ensure all the hydrofluoric acid was removed. Second, metal Ni film was deposited on the prepared Si nanowire at the expense of silicon via a wet displacement deposition process (28−30). Deposition was electrolessly carried out in an alkaline solution containing 1.0 M $NiSO_4$, 2.5 M NH_4F, 0.5 M $(NH_4)_2SO_4$, and 0.01 g of sodium dodecyl sulfate at a temperature of 60 °C, in which the pH value was adjusted to 7.5 by adding NH_4OH. After 5 min, the repeatedly washed samples were immersed in acetone for 1 day to remove the corrosion-resistant plastic layer and dried at 60 °C in vacuum oven. Third, the metal Ni film on Si nanowire was oxidized via thermal treatment at 450 °C for 30 min in a horizontal tube furnace. Before and after oxidation reaction, the sample mass was carefully weighed by an electronic analytical balance so as to calculate the weights of NiO.

2.2. Characterization and Electrochemical Test. The mass of NiO deposited on the Si nanowire array films from low doped-Si wafer with Ni deposition time of 5 and 7 min was estimated to be about 3.0 and 3.73 mg, respectively. The crystal structures of the as-prepared samples were determined by X-ray diffraction (XRD) using the Cu Kα radiation. The morphologies and structures of the samples were characterized using scanning electron microscopy (SEM, JEOL, JSM-6360) and transmission electron microscopy (TEM, JEM2100) equipped with an EDAX PV7715/89 ME energy dispersive X-ray spectrometer (EDS) and selected area electron diffraction (SAED). Electrochemical lithium storage performances of the samples were evaluated by galvanostatic discharge/charge between 0.15 and 3.0 V with the current density of 50 mA/g in a computer controlled battery tester. NiO coated Si nanowire array films were used as working electrode, and Si substrate was used as current collector; Celgard2400 polypropylene foil was as the separator. Lithium metal foil was used as the counter and reference electrodes. The electrolyte solution was 1 M $LiPF_6$ dissolved in ethylene carbonate/diethyl carbonate (EC/DMC, 1:1 by volume). Coin cells were assembled in a glovebox filled with argon atmosphere. All measurements were performed at room temperature.

3. RESULTS AND DISCUSSION

Figure 1a,b depicts typical top-view and cross-section SEM images of as-prepared Si nanowire array film. The diameters of the Si nanowires range from 30 to 300 nm. It can be seen from the cross-sectional SEM that the thickness of the film is about 57 μm and the axes direction of the nanowires is along the direction normal to the original silicon wafer, which is the (100) direction. Typical TEM images of the Si nanowires are shown in Figure 1c,d. The plane spacings in the high resolution TEM (HRTEM) images (Figure 1d) were measured to be 3.1 and 2.7 Å, which can be indexed as $(1\bar{1}1)$ and (002) lattice planes of silicon, respectively. The results indicate that the prepared nanowires are of single crystalline and the axes direction of the nanowires is along the (100) direction of silicon crystalline.

The results of XRD shown in Figure 2a indicate that Si nanowires were coated with NiO after depositing Ni with 5 min on electroless-etched Si nanowires and subsequently annealing with 30 min. Besides the diffraction peak of Si (400) at 69.7°, several diffraction peaks at 37.24°, 43.32°, 62.84°, 75.42°, and 79.46° were observed, which can be

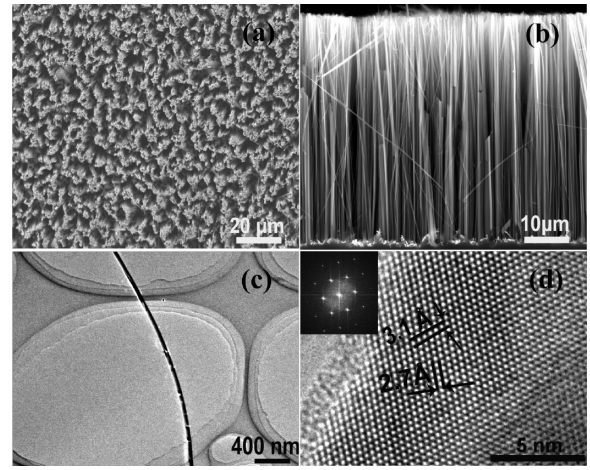

FIGURE 1. (a, b) Typical top-view and cross-sectional SEM images of as-prepared 57 μm long Si nanowire array film, respectively, demonstrating vertical alignment and high density. (c, d) Typical TEM and HRTEM images of single Si nanowire, respectively. The inset in (d) shows the corresponding FFT pattern.

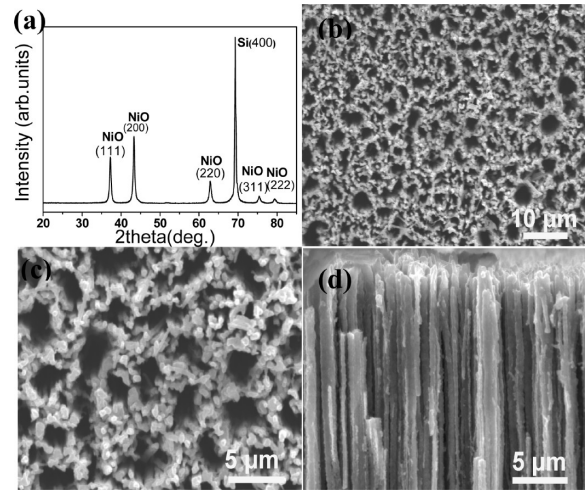

FIGURE 2. (a) Typical XRD patterns of as-prepared 57 μm long NiO coated Si nanowire array film. (b, c, d) Corresponding low-magnification top-view, high-magnification top-view, and cross-section SEM images, respectively.

indexed to the (111), (200), (220), (311), and (222) planes of the cubic NiO phase, respectively. The calculated lattice parameter of NiO is $a = 4.179$ Å, which is in good agreement with the standard value of 4.172 Å (JCDF card no.78-0423). Clearly, no other diffraction peak of metal Ni was detected, implying that the electrolessly deposited Ni was oxidized completely. Figure 2b−d displays typical SEM images of NiO coated Si nanowire array film. The top-view and the cross section morphologies together demonstrate that every Si nanowire is almost uniformly wrapped by a rougher layer of NiO nanoparticles, resulting in NiO coated Si nanowire array films displaying more compact.

The morphology and microstructure of the as-prepared NiO coated Si nanowire array films were further examined by TEM observations. Figure 3a shows a typical low-magnified TEM image of individual NiO coated Si nanowire. A rough layer of NiO nanoparticles can be seen. The corresponding SAED pattern (see Figure 3c) contains polycrystalline rings besides sharp diffraction points of crystalline Si.

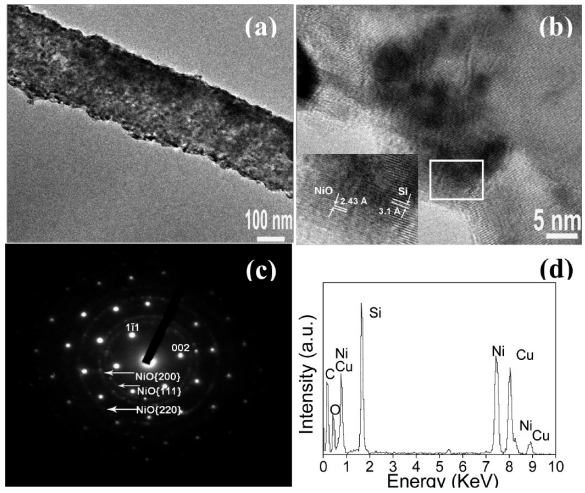

FIGURE 3. (a) Typical TEM image of as-prepared NiO coated Si nanowires from low doped-Si wafer with Ni deposition time of 5 min. (b, c) The corresponding SAED pattern and HRTEM images, respectively. The inset in (b) is the magnified image of the marked section. (d) EDS spectrum of singed NiO coated Si nanowire.

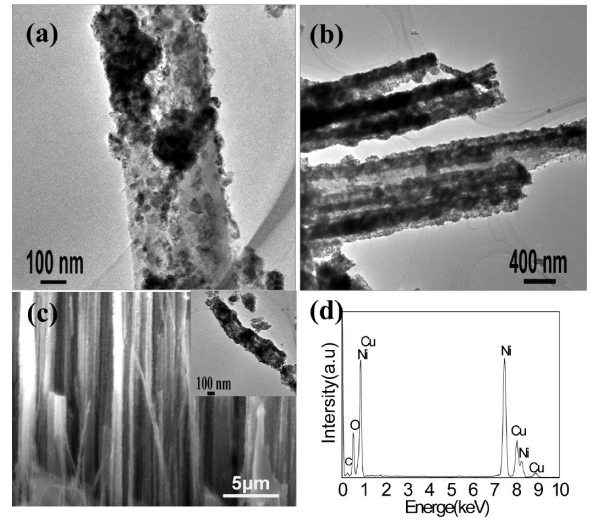

FIGURE 4. (a, b) Typical TEM images of as-prepared NiO coated Si nanowires from low doped-Si wafer with Ni deposition time of 3 and 10 min, respectively. (c, d) Typical SEM image and EDS spectrum of as-prepared NiO nanowire arrays from highly doped-Si wafer with Ni deposition time of 5 min. The inset in (c) is a typical TEM image of NiO nanowire.

These diffraction rings can be well indexed to the (111), (200), and (220) lattice plane of cubic NiO phase. The HRTEM image as shown in Figure 3b is blurrier than that of Si nanowires due to a thin NiO layer. Nevertheless, the lattice fringes of the NiO (111) and Si ($1\bar{1}1$) planes can be seen, demonstrating clearly that the crystalline NiO was coated on the surface of Si nanowire. Further EDS measurement (see Figure 3d) reveals that individual NiO coated Si nanowire consists of silicon, nickel, and oxygen. The atom contents of Ni and O are 13.29% and 12.7%, respectively, which is close to the formula of NiO.

In our experiments, metal Ni to form the NiO layer was deposited on the prepared Si nanowire at the expense of silicon via a process known as displacement deposition (28−30). Therefore, Ni deposition time and doping concentration in silicon have great influence on the structure and composition of final NiO coated Si nanowire. Figure 4a,b displays typical TEM images of as-prepared NiO coated Si nanowires from low doped-Si wafer with Ni deposition time of 3 and 10 min, respectively. It is clearly displayed that the outer NiO shell is too thin to completely wrap Si core for the former, while for the latter, the NiO shell is rather thick and the inner Si cores are etched to some degree. Figure 4c shows a typical SEM image of the nanowire array film obtained from highly doped Si wafer with Ni deposition time of 5 min and subsequently annealing with 30 min, displaying no obvious morphology difference compared with that from low doped Si wafer. However, TEM observation (see the inset in Figure 4c) indicates that the nanowire is fragile and its surface is seriously rough. Further EDS measurement as shown in Figure 4d reveals the sample consists of nickel and oxygen besides carbon and cuprum from a C-coated Cu TEM grid. No obvious Si was detected via EDS measurement, implying that most of the Si have been replaced by nickel to form NiO nanowire array films. In fact, similar phenomena that Si can be completely replaced by nickel had also been reported in previous works by Zhang et al (29, 30). They successfully prepared hierarchical porous nickel from macroporous silicon through increasing the time of displacement deposition. This unexpected result would likely be attributed to the fact that higher doping concentration in Si nanowires lowers the energy barrier to charge injection across the silicon surface, resulting in the speedup of displacement deposition between silicon atom and Ni atom (31, 32).

Recently, silicon-based nanostructured materials for lithium-ion battery anodes have attracted tremendous interest, owing to the fact that silicon has extremely high theoretical specific capacity of about 4200 mAh/g (19, 20, 24, 26, 33, 34). However, the contribution of silicon wafer substrate could not be excluded from the capacity of the anode NiO coated Si nanowire array films. If the potential window versus lithium is adjusted beyond 0.150 V during the galvanostatic charge/discharge tests, the reaction of Si with lithium at 120 mV would be limited (19, 33, 35), resulting in only coated NiO being utilized as active materials for lithium storage and release, while highly conductive crystalline Si nanowire core acting as mechanical support and electron transport pathways due its maintained structural integrity and attachment to Si wafer. Figure 5a shows the galvanostatic charge/discharge performances of NiO coated Si nanowire array film obtained from low-doped silicon wafer with Ni deposition time of 5 min at the current density of 50 mA/g in the potential range of 0.150−3.0 V. During the first discharge, a plateau at 0.7 V, followed by a gradual slope, can be observed. Subsequent charge curve shows a large voltage hysteresis, indicating a conversion mechanism instead of intercalation mechanism of the conventional carbonaceous materials (8). The total capacity of the samples for the first discharge reaches 1116.37 mAh/g. A capacity of 842.59 mAh/g is delivered for the first charge process. NiO coated Si nanowire array film electrodes show a Coulombic efficiency of 75.75%, and the corresponding irreversible capacity loss (ICL) value is 273.78 mAh/g. The NiO coated

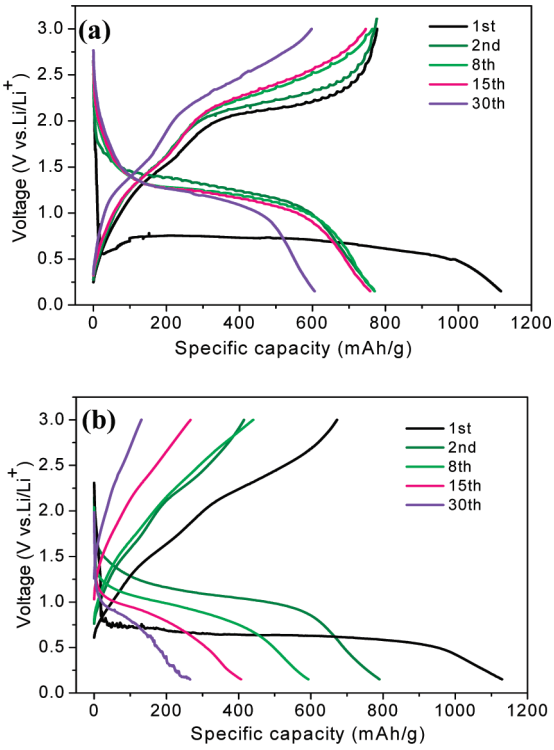

FIGURE 5. Charge−discharge curves of (a) NiO coated Si nanowire array film from low doped-Si wafer with Ni deposition time of 5 min and (b) NiO nanowire array film from highly doped-Si wafer at the current density of 50 mA/g in the potential range of 0.150−3.0 V.

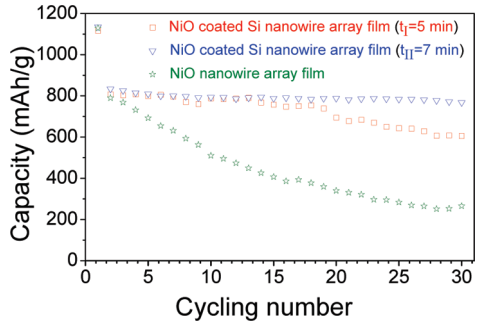

FIGURE 6. Cyclic performance comparison of NiO nanowire array film and NiO coated Si nanowire array films with different Ni deposition times ($t_I = 5$, $t_{II} = 7$ min).

Si nanowire array film reported here shows a reversible capacity close to 2.39 times of the graphite (372 mAh/g). However, according to the conversion reaction of nickel oxide with lithium (8): $NiO + 2Li^+ + 2e^- \leftrightarrow Ni + Li_2O$, the discharge process should consume 2.0 Li per Ni. Hence, the high capacity of the initial discharge and charge process might be caused by both the formation of solid electrolyte interface (SEI) film and the polymeric gel-type layer on the material resulting from the solvent decomposition of the electrolyte (6, 8). In addition, the NiO coated Si nanowire array film electrode exhibits superior cycling properties as shown in Figure. 6. The reversible capacity of 606.13 mAh/g is obtained when the cell is cycled at a rate of 50 mA/g after the 30th cycle.

For comparison, the NiO nanowire film electrode obtained from highly doped Si wafer was also measured, and the results are also displayed in Figures 5 and 6. The first discharge capacity of the NiO nanowire film electrode is 1129.29 mAh/g, and the corresponding ICL value is 366.23 mAh/g. The Coulombic efficiency of the first cycle is 67.2%, which is 8.5% lower than that of the NiO coated Si nanowire array film electrode. Furthermore, the NiO nanowire film electrode exhibits poor cyclability, and the discharge/charge capacity decreases sharply in subsequent cycling. The reversible capacity obtained after the 30th cycle is 265.1 mAh/g, which is much lower than that of NiO coated Si nanowire film. The severe capacity degradation and poor cycling performance should be attributed to the poor electronic conductivity and large structure and volume changes during Li^+ ion insertion and extraction (6, 8). In fact, the first reversible capacity and cycling characteristics of NiO layer on Si nanowires are also comparable to those reported in NiO nanostructures under the same conditions (12, 13). Considering the hybrid structure characteristics, the improved capacity and cycle life of NiO coated Si nanowire array film likely benefit from improved conductivity provided by highly conductive Si nanowires in the inner core and well-directed conductive paths due to perfect array alignment. The two factors facilitate electron transport to the NiO shell. In addition, the active shell of NiO nanoparticles decreases the effective ion diffusion path and increases the surface area for insertion and extraction of lithium to improve its electrochemical performance. Moreover, the cycling properties of NiO coated Si nanowire arrays obtained from low doped-Si wafer with Ni deposition time of 7 min were also measured (See Figure 6). The results reveal that its cycling performance is even superior. Hence, it can be inferred that there must exist an optimal Ni deposition time to prepare NiO coated Si nanowire arrays.

4. CONCLUSIONS

In summary, highly ordered NiO coated Si nanowire array films were prepared via depositing Ni on electroless-etched Si nanowires and subsequently annealing. Electrochemical tests indicate that, by controlling potential window versus lithium, the coated NiO can be selected to be electrochemically active to store\release Li^+ ions, while highly conductive crystalline Si cores function as nothing more than a stable mechanical support and an efficient electrical conducting pathway. Compared to NiO nanostructured anode materials, the NiO coated Si nanowire array films exhibit large lithium storage capacity, high Coulombic efficiency, and superior cycling properties, implying that they have promising application for anode materials in rechargeable lithium-ion batteries.

Acknowledgment. This work was supported by the grants from National Natural Science Foundation of China (Nos. 10802071 and 10774127), the Cultivation Fund of the Key Scientific and Technical Innovation Project (708068), Ministry of Education of China, the Doctoral Program of Higher Education (No. 2008053 00003), and the Open Fund based on the innovation platform of Hunan colleges and universities (No. 09K033).

REFERENCES AND NOTES

(1) Aricò, A.; Bruce, P.; Scrosati, B.; Tarascon, J.; Van Schalkwijk, W. *Nat. Mater.* **2005**, *4*, 366.
(2) Chung, S.; Bloking, J.; Chiang, Y. *Nat. Mater.* **2002**, *1*, 123.
(3) Guo, Y.; Hu, J.; Wan, L. *Adv. Mater.* **2008**, *20*, 2878.
(4) Armand, M.; Tarascon, J. *Nature* **2008**, *451*, 652.
(5) Leroux, F.; Goward, G.; Power, W.; Nazar, L. *Electrochem. Solid-State Lett.* **1998**, *1*, 255.
(6) Poizot, P.; Laruelle, S.; Grugeon, S.; Tarascon, J. *J. Electrochem. Soc.* **2002**, *149*, A1212.
(7) Tarascon, J.; Armand, M. *Nature* **2001**, *414*, 359.
(8) Poizot, P.; Laruelle, S.; Grugeon, S.; Dupont, L.; Tarascon, J. *Nature* **2000**, *407*, 496.
(9) Li, W.; Xu, L.; Chen, J. *Adv. Funct. Mater.* **2005**, *15*, 851.
(10) Li, Y.; Tan, B.; Wu, Y. *Nano Lett.* **2008**, *8*, 265.
(11) Nam, K.; Kim, D.; Yoo, P.; Chiang, C.; Meethong, N.; Hammond, P.; Chiang, Y.; Belcher, A. *Science* **2006**, *312*, 885.
(12) Needham, S.; Wang, G.; Liu, H. *J. Power Sources* **2006**, *159*, 254.
(13) Pan, Q.; Liu, J. *J. Solid State Electrochem.* **2009**, *13*, 1591.
(14) Reddy, M.; Yu, T.; Sow, C.; Shen, Z.; Lim, C.; Rao, G.; Chowdari, B. *Adv. Funct. Mater.* **2007**, *17*, 2792.
(15) Taberna, P.; Mitra, S.; Poizot, P.; Simon, P.; Tarascon, J. *Nat. Mater.* **2006**, *5*, 567.
(16) Varghese, B.; Reddy, M.; Yanwu, Z.; Lit, C.; Hoong, T.; Rao, G.; Chowdari, B.; Wee, A.; Lim, C.; Sow, C. *Chem. Mater.* **2008**, *20*, 3360.
(17) Wang, X.; Li, L.; Wang, S.; Zhang, Z.; Fei, L.; Qian, Y. *Cryst. Growth Des.* **2006**, *6*, 2163.
(18) Zou, G.; Li, H.; Zhang, D.; Xiong, K.; Dong, C.; Qian, Y. *J. Phys. Chem. B* **2006**, *110*, 1632.
(19) Cui, L.; Ruffo, R.; Chan, C.; Peng, H.; Cui, Y. *Nano Lett.* **2008**, *9*, 491.
(20) Cui, L.; Yang, Y.; Hsu, C.; Cui, Y. *Nano Lett.* **2009**, *9*, 3370.
(21) Kim, H.; Cho, J. *Nano Lett.* **2008**, *8*, 3689.
(22) Reddy, A.; Shaijumon, M.; Gowda, S.; Ajayan, P. *Nano Lett.* **2009**, *9*, 1002.
(23) Wang, W.; Kumta, P. *ACS Nano* **2010**, *4*, 2233.
(24) Huang, R.; Fan, X.; Shen, W.; Zhu, J. *Appl. Phys. Lett.* **2009**, *95*, 3119.
(25) Peng, K.; Huang, Z.; Zhu, J. *Adv. Mater.* **2004**, *16*, 73.
(26) Peng, K.; Jie, J.; Zhang, W.; Lee, S. *Appl. Phys. Lett.* **2008**, *93*, 033105.
(27) Peng, K.; Yan, Y.; Gao, S.; Zhu, J. *Chem.—Eur. J.* **2002**, *6*, 413.
(28) Jiang, P.; Cizeron, J.; Bertone, J.; Colvin, V. *J. Am. Chem. Soc.* **1999**, *121*, 7957.
(29) Zhang, X.; Tu, K. *J. Am. Chem. Soc.* **2006**, *128*, 15036.
(30) Zhang, X.; Tu, K.; Xie, Y.; Tung, C.; Xu, S. *Adv. Mater.* **2006**, *18*, 1905.
(31) Cullis, A.; Canham, L.; Calcott, P. *J. Appl. Phys.* **1997**, *82*, 909.
(32) Oskam, G.; Long, J.; Natarajan, A.; Searson, P. *J. Phys. D: Appl. Phys.* **1998**, *31*, 1927.
(33) Chan, C.; Peng, H.; Liu, G.; McIlwrath, K.; Zhang, X.; Huggins, R.; Cui, Y. *Nat. Nanotechnol.* **2007**, *3*, 31.
(34) Teki, R.; Datta, M.; Krishnan, R.; Parker, T.; Lu, T.; Kumta, P.; Koratkar, N. *Small* **2009**, *5*, 2236.
(35) Limthongkul, P.; Jang, Y.; Dudney, N.; Chiang, Y. *Acta Mater.* **2003**, *51*, 1103.

AM100791Z